



Remote sensing analysis for surface urban heat island detection over Jeddah, Saudi Arabia

Yehia H. Miky^{1,2} 

Received: 29 April 2018 / Accepted: 31 January 2019 / Published online: 14 February 2019
© Società Italiana di Fotogrammetria e Topografia (SIFET) 2019

Abstract

Urbanization and human activity within an urban system produce many destructive and irreversible effects on natural environment such as air pollution and climate changes. One of the important effects of climate change is the formation of surface urban heat island (SUHI) which is an area with higher temperature than surroundings. It is important to study the surface urban heat islands to understand the complexity of the climate systems and to lessen their impact on the environment. In this paper, an approach for detecting SUHIs based on the combination between a set of Landsat 8's Thermal Infrared Sensor (TIRS) night vision images and Spot5 data was proposed. To accurately detect SUHIs over Jeddah City, it is important to determine the land surface temperature (LST). To achieve this goal, pixel values of Landsat images were converted to represent at sensor temperature. The spot image was classified using supervised classification techniques to determine feature types in the scene, the emissivity value for each pixel was assigned using classification-based emissivity and NDVI-based emissivity. Then, the two values of at sensor temperature and feature emissivity were linked together to retrieve an accurate LST. Based on the results of this study, the SUHIs over Jeddah City appeared as small boundaries in the South area of the city, as a result of the land use patterns. The difference between urban and non-urban areas ranges from 4 to 7 °C. The SUHIs over Petromin neighborhood and Almohajer neighborhood were presented. Night vision Landsat 8 offers an effective framework to delineate and monitor behavior, movement, and size of SUHIs. The early detection of SUHIs by remote sensing data contributes in discovering environmental imbalance and helps to identify problems and developing solutions.

Keywords SUHI · Thermal remote sensing · Land surface emissivity

Introduction

Temperature is one of the most crucial climate elements. It has a significant impact on different human activities (such as agriculture, housing, and tourism). Regarding the close relationship between temperature and climate elements, the temperature is considered as the engine for the rest of the other climate elements. These elements mainly affect each other. Human activity within an urban system produces many destructive and irreversible effects on natural environments. The human effect can be noticed through pollution of the seas and

oceans, the pollution of atmosphere, logging, building cities with high towers, and other interventions that might show their effect on climate patterns over the long run. The effect on climate may be through several variables and factors that are integrated to form an area with higher temperature than surrounding areas, which is called urban heat island (UHI). In fact, the increase in urban activities in modern cities has a significant influence on climate change, which leads to more UHIs (Salleh et al. 2013).

Urbanization can be defined as the process of changing the region characteristics, mainly due to the human activities (Sinasi et al. 2012). These changes may affect the land surface or the local climate in that regions. The main cause of the climate change in urban areas is the biophysical features of the urban areas that amplify the effect of the climate change over these areas (Fortuniak 2009). Due to the mandatory effect of urbanization and population growth on the thermal properties of the surroundings, several studies regarding the thermal properties change, their types, and factors affecting them were

✉ Yehia H. Miky
yhassan@kau.edu.sa

¹ Department of Geomatics, Faculty of Environment Design, King AbdulAziz University, Jeddah, Saudi Arabia

² Faculty of Engineering, Aswan University, Aswan, Egypt

done. According to (Brazel et al. 2000), there is a modification of the radiative fluxes because of changing natural land into man-made objects. This thermal change of the surface properties is mainly due to multiple reflections and dislocation of the solar radiation and hydrologic balance. These factors increase the urban-rural contrast in air temperature and surface radiance of that urbanized area. The difference in the air temperature between an urban area and its surrounding is called urban heat island (Oke 1987). According to (Ward 2008), an urban heat island is a metropolitan area which is significantly warmer than its surrounding areas. UHI plays a crucial role in climatic change; it has been commonly associated to most cities and it is considered as an alarming climatic phenomenon that requires deep investigations. UHI has been copiously addressed in the last few years in urban areas with a wide range of landscapes and different climate conditions.

Urban heat island types

UHI may be classified into two main types: i) surface urban heat islands, and ii) atmospheric urban heat islands (Bhargava et al. 2017; Parlow et al. 2014).

Surface urban heat islands Surface urban heat island, SUHI, namely remotely sensed urban heat island, is usually visualized as a dome of hot air over urban areas with the help of far infrared data that allow to retrieve land surface temperature (LST). Using remote sensing, the urban land cover explains the SUHI intensities of many European cities (Zhou et al. 2013). Oke (1982) stated that surface urban heat islands occurred at night as same as at daytime but seemed to be stronger at night than they are at daytime. Dry exposed urban surfaces like roads and roofs can be heated to a temperature hotter than that for the air, while in moist surfaces the temperature of the air is usually close to the surface temperature (Berdahl and Bretz 1997). As it would be expected in most regions, the SUHI is usually greater in summer than they are in the other seasons as a result of changing in solar radiation and the drier weather Conditions (Oke 1987). The differences in nighttime, SUHI temperatures between urban and non-urban areas are typically 10 to 15 °C, considered higher than the daytime differences which is 5 to 10 °C (Voogt and Oke 2003).

Atmospheric urban heat islands The atmospheric urban heat islands may be described as the comparison between warmer air and cooler air in nearby rural areas, which can be divided into two main types: 1) canopy layer urban heat islands and 2) boundary layer urban heat islands. Canopy layer urban heat island exists in the lowest air layer, where people live, and extends from the ground surface to below the tops of urban roofs and vegetation. Boundary layer urban heat island begins from the urban roofs and extends up to the point where there is no urban effect of the atmosphere, usually 1.5 km from the

surface (Li et al. 2012). The effect of atmospheric UHI during the daytime is absent and after sunset shows features similar to the nighttime SUHI (Bonafoni et al. 2015). Atmospheric urban heat island mainly relies on ground-based in-situ measurements of air temperature and can be considered the classical way of assessing the urban heat islands (Parlow et al. 2014). It is absolutely necessary that technical terms of urban heat islands are clearly separated because UHI and SUHI are mostly decoupled during daytime (Oke et al. 2017).

Factors influencing affecting urban heat islands

The formation of UHI is determined by several factors, such as geographical location, size and function of the city, building material properties, synoptic weather, and time. Changing the land use and reducing vegetation is one of the most important factors leading to the growth and development of thermal islands, which are formed mainly in cities (He et al. 2007). The thermal island generated over the city depends mainly on the total area covered by materials with high capacity to absorb and storage the heat such as asphalt, brick, concrete, and stone. Most of these materials do not have a good reflectivity, that is, the proportion of reflected radiation is relatively low (Abutaleb et al. 2015). In addition, the compaction of soils under roads not only increases their carrying capacity, but also increases their heat storage capacity (Abu-Hamdeh 2003). In fact, most modern cities are famous for multi-story buildings surrounded by tiled areas, these high buildings tend to catch the sun, so that the heat generated from these buildings increase in the spaces between them, and this helps in a session on the city's temperature rise.

Land surface temperature and emissivity retrieval methods

The emissivity of a material can be defined as the ratio of the radiance emitted from this material to that radiance emitted by a black body at the same temperature and wavelength (Li et al. 2013). However, the emissivity of land, unlike that of oceans, can differ significantly from the emissivity of the black body which equals one and vary with vegetation, surface moisture, roughness, and viewing angles (Salisbury and D'Aria 1992). Satellite sensors can measure radiance covering a wide range of the spectral. Land surface emissivity (LSE) can be estimated with the help of the collecting radiance which contains the combined effects of surface and atmosphere. Several methods have been produced to retrieve LSE from remotely sensed data, each has its advantages and limitation. The most proper methods are 1) semi-empirical method, 2) multi-channel emissivity method, and 3) physically based method (Zhou et al. 2013). Although all these methods use assumptions based on Planck's law and can be used effectively to get LSE, each method has its own procedure. Semi-empirical methods

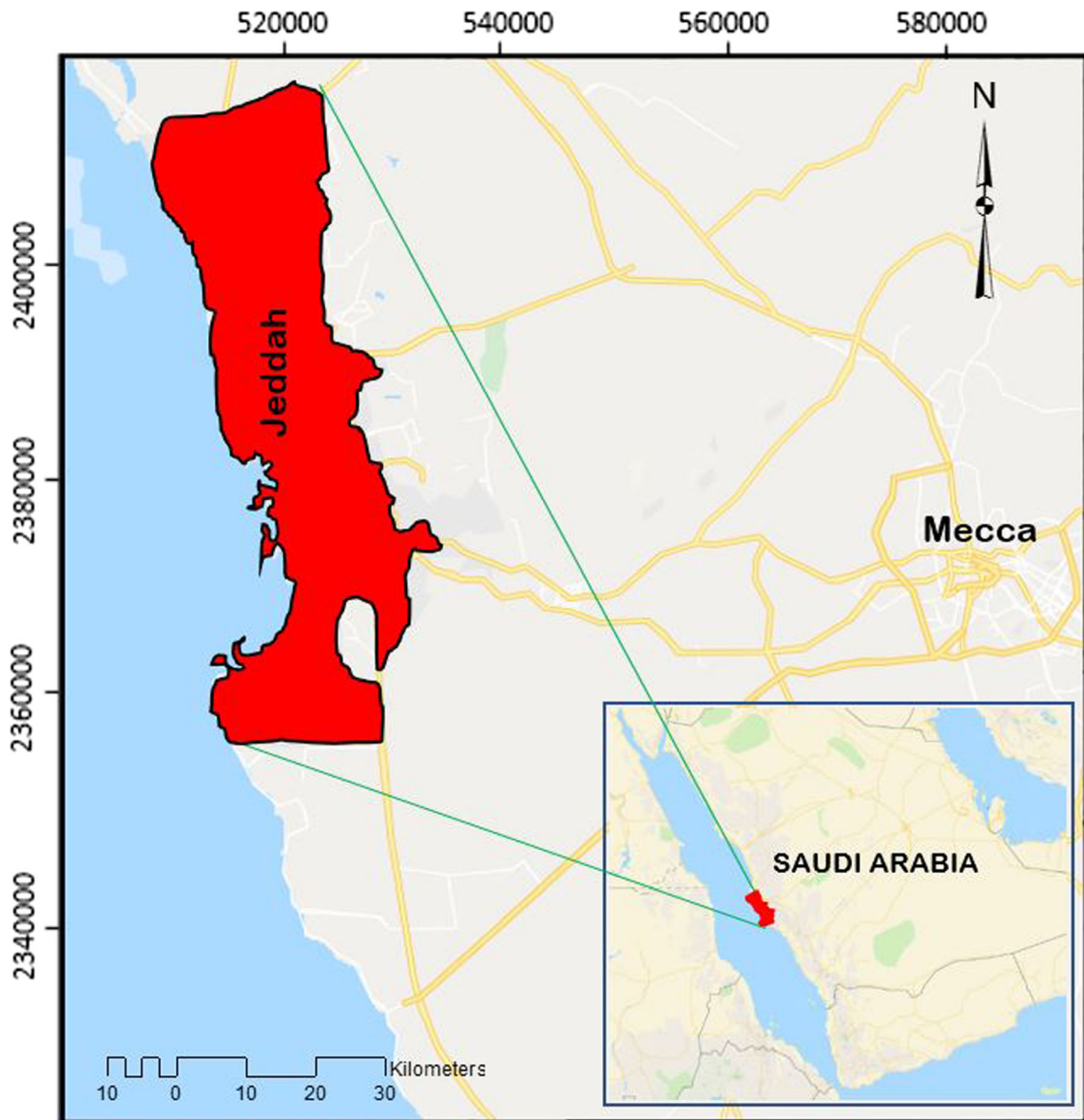


Fig. 1 Location of Jeddah city in the west of Saudi Arabia

include classification-based emissivity method (CBEM) (Peres and Da Camara 2005; Snyder et al. 1998) and normalized difference vegetation index (NDVI)–based emissivity method (NBEM) (Sobrino and Raissouni 2000; Van de Griend and

Owe 1993). In classification-based emissivity method, conventional classification is used and then emissivity can be assigned related to the land cover. Snyder et al. (1998) proposed CBEM to determine LST from the thermal band of the

Table 1 Landsat 8 datasets acquired for Jeddah region

Scene ID	Acquisition date	Scene_center time	Sun_Azimuth angle	Day/night indicator
LC80391992015173LGN01	22 June 2015	19:20:20.95	270.5140188	Night
LC80391992015189LGN01	08 July 2015	19:20:31.10	269.1143650	Night
LC80391992015205LGN02	24 July 2015	19:20:37.70	320.7815614	Night
LC81700452016006LGN03	06 Jan. 2016	07:49:14.36	149.6146895	Day
LC81700452016054LGN01	23 Feb. 2016	07:49:03.86	137.3348050	Day
LC81700452016070LGN01	10 Mar. 2016	07:49:02.04	131.7523560	Day

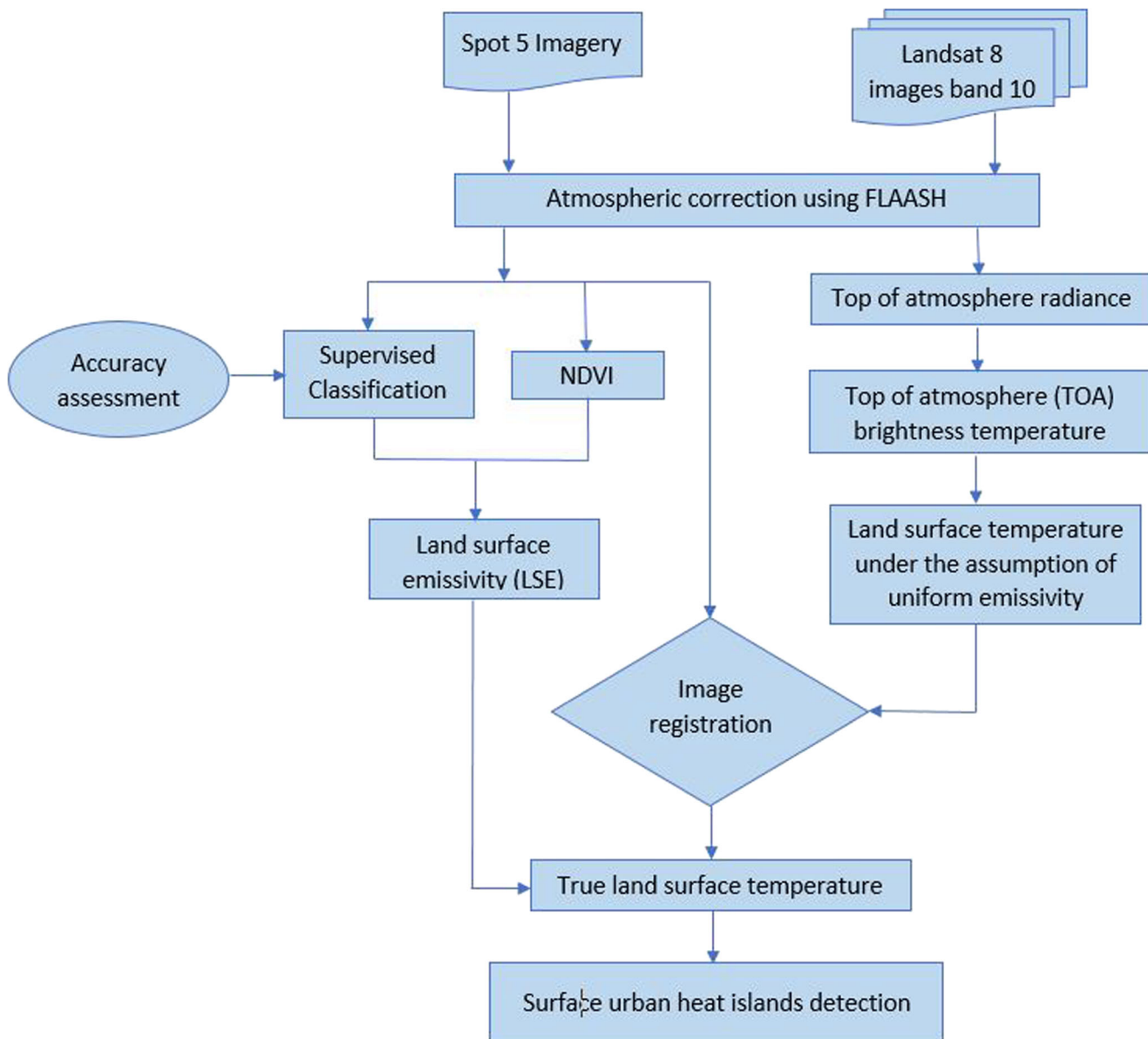


Fig. 2 A typical workflow of the proposed methodology

moderate resolution image spectroradiometer (MODIS TIR). They developed the emissivity database using spectral laboratory measurements derived from samples of materials. The results indicated that almost 70% of the earth’s land surface emissivity can be determined with an accuracy sufficient to meet the goal of an accuracy of 1 K required for MODIS LST calculation.

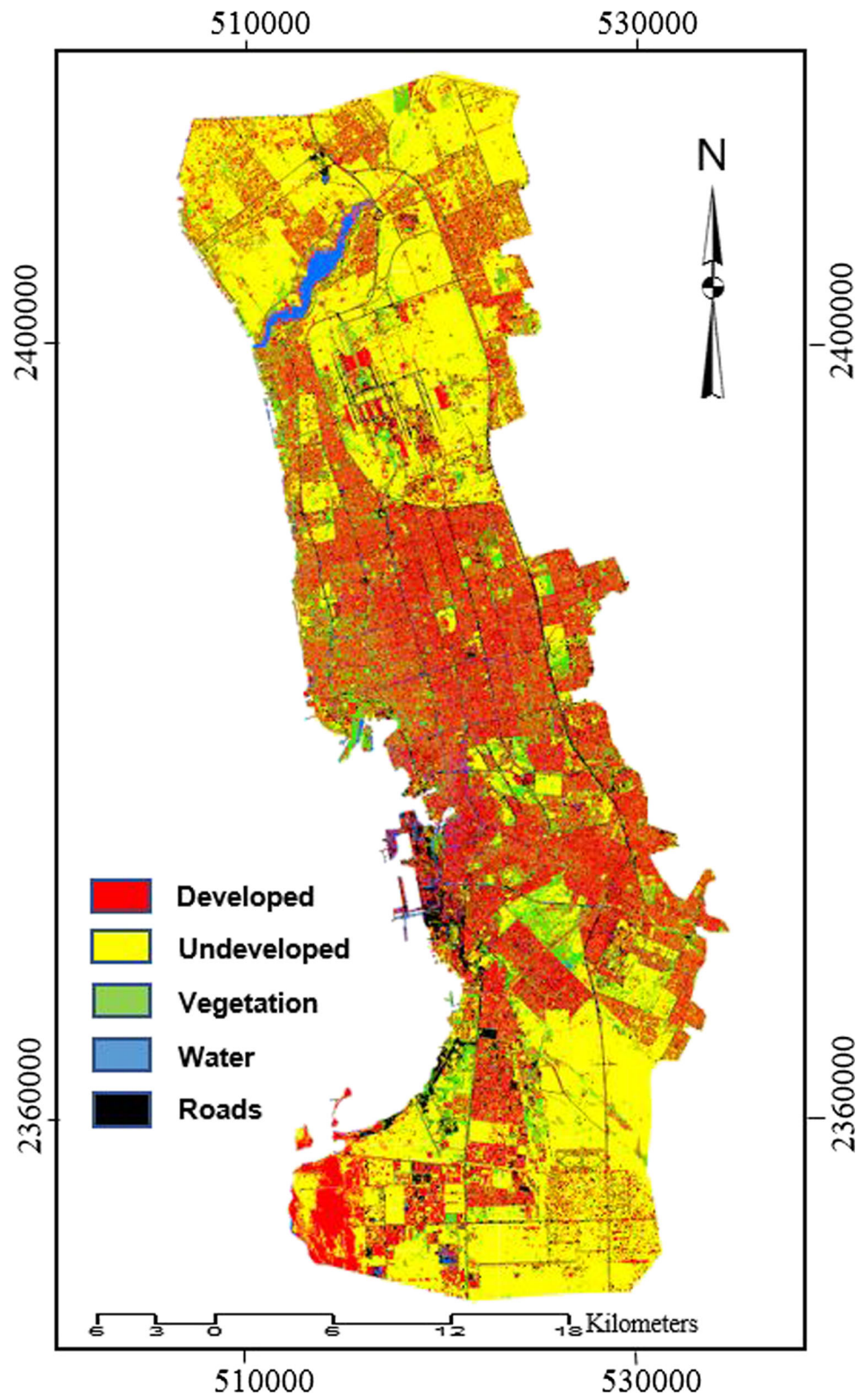
The emissivity calculation based on NDVI was proposed by Van de Griend and Owe (1993) when they found a high

correlation between the band covering 8–10 μm and the logarithm of the NDVI. In multi-channel methods, the LSE can be retrieved directly from the emitted spectral radiance after considering some assumptions and constrains. For example, the gray-body emissivity (GBE) method, presented by Barducci and Pippi (1996), assumed that the emissivity for wavelengths larger than 10 μm has a flat spectrum while the two-temperature method (TTM) assumed that the emissivity at a channel is time invariable (Watson 1992). However, the iterative spectrally smooth temperature emissivity separation (ISSTES) method proposed by Borel (1997) assumed that the emissivity spectrum is smooth. Reference channel method (RCM) is considered as the simplest method for emissivity retrieval from the space because it assumes that the emissivity in one channel is constant and has the same value for all pixels (Kahle et al. 1980).

Table 2 Emissivity values assigned for each class after classification

Roads	Urban areas	Agricultural	Water	Bare soil
0.974	0.953	0.983	0.990	0.959

Fig. 3 Supervised classification of Jeddah city using maximum likelihood classifier



Unlike the semi-empirical methods and multi-channel methods, physically based methods consider the physical effect of atmosphere due to the spectral emission and absorptions.

Temperature-independent spectral indices (TISI) method first proposed by Becker and Li (1990) is one of the physically based method due to the assumption that the spectral radiance emitted

Table 3 The error matrix for the supervised classification for spot 5 satellite image of Jeddah city, KSA

Classified category	Actual category						User's accuracy
	Water	Vegetation	Roads	Urban	Undeveloped	Total	
Water	22	0	0	0	0	22	100.00%
Vegetation	0	33	0	0	0	33	100.00%
Roads	0	0	24	0	1	25	96.00%
Urban	0	2	2	83	2	89	93.26%
Undeveloped	0	0	0	9	16	25	64.00%
Total	22	35	26	92	19	194	
Producer's accuracy	100.00%	94.28%	92.31%	90.22%	84.21%		

Overall classification accuracy = 91.75%. Overall kappa = 0.884

from the land in MIR band is equal to the reflected spectral radiance if the surface reflectance in this channel is about 0.1 and there is no reflection in the night. So, the idea here is to eliminate the emitted radiation during the day with that of during the night (Li et al. 2000). The physics-based day/night operational method was proposed to retrieve the LSE in semi-arid and arid regions, using day/night pairs of combined MIR and TIR data (Wan and Li 1997). Also, the two-step physical retrieval method (TSRM) is one of the physically based methods, which based on the atmospheric profile retrieval and use of the principal component analysis (PCA) technique to reduce the number of unknowns (Li et al. 2007; Ma et al. 2000).

The study of SUHI is useful in the field of development and regional planning. As it accelerates solutions for problems in the human environment, the use of technology in detecting and monitoring environmental changes such as SUHI is very important. Also, understanding thermal islands and their behavior in the city help us to take measures to improve the development of the city's financial budgets, which can be done by rationalizing the use of energy resulting from the exacerbation of thermal islands phenomenon of the city and identifying ways to optimize the use of environmental resources and entertainment in the city under the thermal characteristics. So, it is important to study the surface urban heat islands to understand the complexity of the climate systems and to lessen their impact. The main objective of this study is to use remotely sensed data to detect SUHIs over Jeddah city, Saudi Arabia.

Methodology

Study area

Jeddah is the second largest city in Saudi Arabia. It has a population of approximately 3.45 million (around 14% of the total population of the Kingdom). It is located in the west coast of Saudi Arabia at latitude 29.21° north and longitude 39.7° east as shown in Fig. 1. The total area of Jeddah municipality is

5460 km²; therefore, its urban area is 1765 km² which lies from the coast to 15 km towards the east. According to Ministry of Municipality and Rural Affairs report, land use in Jeddah went through remarkable changes during last decades. Although all land uses changed from 1964 until now, five significant land use classes have rapidly and actively changed: residential, commercial, industrial, informal settlements, and public spaces. Among these classes, residential development has dramatically increased, and the number of dwellings reached about 900,000 dwellings (Future Saudi cities, Jeddah CPI profile 2018). Generally, Saudi Arabia has a desert climate with extreme heat during the day, an abrupt drop in temperature at night, erratic rainfall. Due to the influence of a subtropical high-pressure system and many fluctuations in elevation, there is a considerable variation in temperature and humidity. Furthermore, some areas have different climate, particularly, the area along the coastal regions of the red sea. During winter, the temperature ranges from 15 °C at midnight to 25 °C in the afternoon. While summer temperature is very high, often breaking the mark 40 °C in the afternoon and dropping to 30 °C in the evening.

Satellite imagery and pre-processing

Landsat data, stretched back to 1970s, are uniquely adaptable for ecological studies within urban environment. The archive of data which is freely available gives researchers an uninterrupted record of changes to the earth's surface. As the Landsat scene is repeated every 16 days, this allows for high temporal resolution, with a spatial resolution of 15 m for panchromatic and 30 m for multispectral, has proven sufficient for investigating multiple issues of environmental concern, in particular, the urban heat island location and intensity. Landsat 8's thermal infrared sensor (TIRS) is designed to detect the energy emitted from the surface of the earth, which varies in intensity based on the material composition of the local surface. TIRS is designed to collect infrared radiation that exists at approximately the 10.60 and 12.51 μm wavelengths and passes upward from the earth's surface with little modification or depletion by the gasses of the earth's atmosphere. As

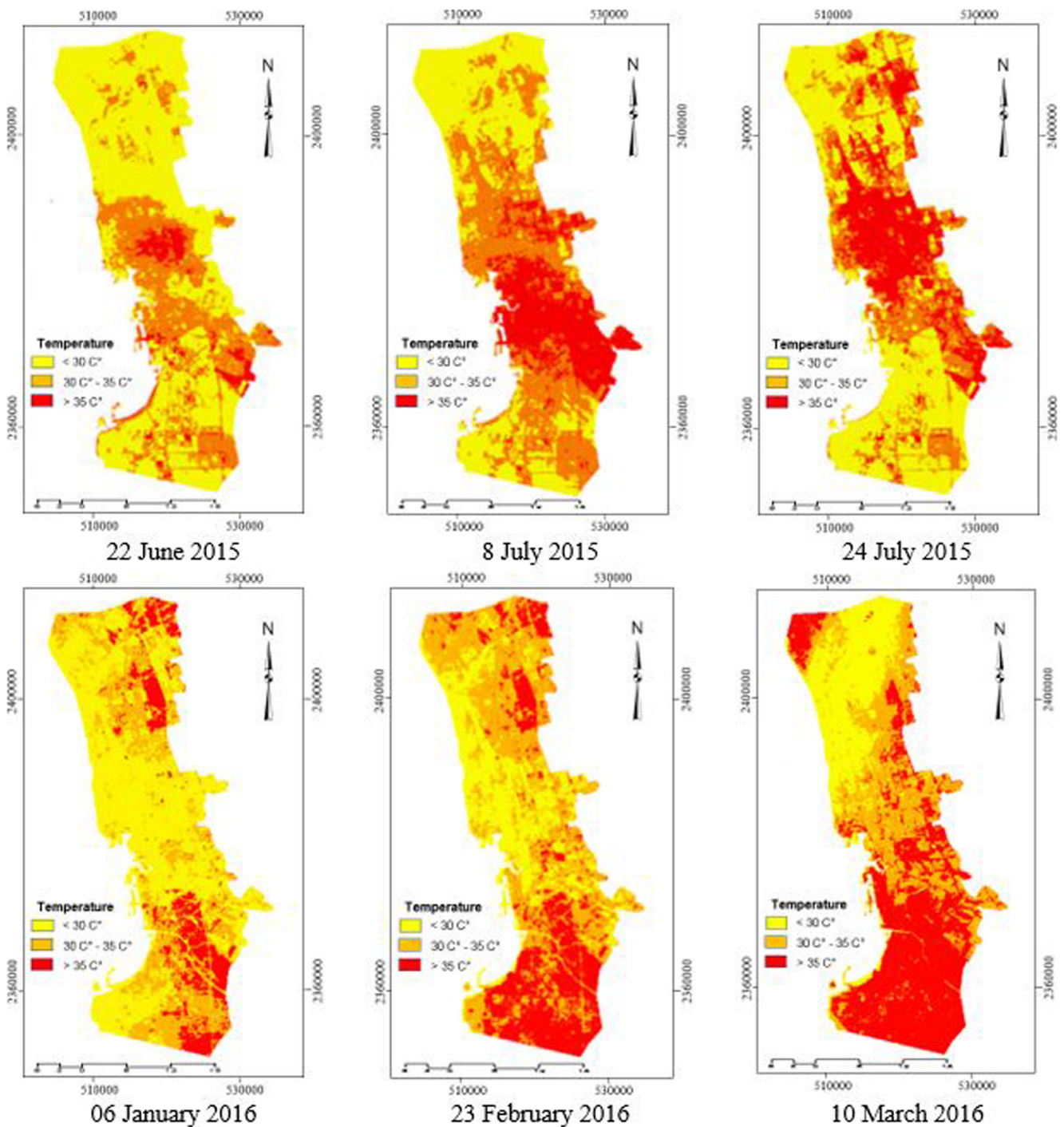


Fig. 4 Land surface temperature over Jeddah city using classification-based emissivity and NDVI-based emissivity values

mentioned in the Landsat 8 User's Handbook, band 11 is significantly more contaminated by stray light than band 10 and only data from band 10 are suitable at the moment for LST retrieval due to the larger uncertainty in the band 11 values (Barsi et al. 2014; Montanaro et al. 2014; United States Geological Survey 2017). Therefore, single channel approach should be used to retrieve LST from Landsat thermal data (Jiménez-Muñoz and Sobrino 2003; Cristóbal et al.

2009, 2018). In this study, we will use only band 10 from Landsat 8 images to retrieve surface temperature. The main purpose of this research is to study the SUHI phenomenon over Jeddah region. To do so, six sets of Landsat 8 Imagery (path/row: 39/199) with Level 1T are used (USGS Global Visualization Viewer 2017). In addition, a spot 5 multi-spectral satellite imagery of the study area acquired at 9 July 2015 are used (Table 1).

Table 4 Land cover temperature (°C) derived from Landsat 8 images

Land cover	Min.	Aver	Max.	S D	Median	NMAD
22 June 2015						
Roads	12.60	23.93	31.23	1.081	24.81	0.743
Urban areas	12.58	23.67	31.17	1.233	24.52	0.907
Agricultural	18.66	23.71	26.94	1.119	23.41	0.887
Water	21.03	23.75	31.20	0.750	23.84	0.446
Bare soil	12.59	23.35	31.23	1.472	23.71	1.079
08 July 2015						
Roads	13.60	24.85	38.80	0.999	25.97	0.779
Urban areas	13.86	24.37	36.84	1.163	25.35	0.851
Agricultural	20.48	24.32	32.71	1.006	25.19	0.740
Water	20.41	23.82	30.57	1.041	24.58	0.679
Bare soil	14.29	23.65	38.84	1.177	24.22	0.881
24 July 2015						
Roads	14.80	25.49	32.45	1.559	27.42	1.182
Urban areas	15.06	25.12	40.86	1.989	27.18	1.745
Agricultural	21.57	25.15	32.18	1.663	27.03	1.345
Water	22.42	24.43	29.40	1.372	25.83	1.041
Bare soil	14.81	24.79	42.63	1.741	25.48	1.439
06 January 2016						
Roads	21.18	27.71	38.11	1.381	27.63	1.232
Urban areas	21.74	27.72	39.74	1.386	27.51	1.115
Agricultural	22.21	27.53	37.23	1.470	26.44	1.232
Water	20.03	24.76	32.32	1.986	24.51	1.681
Bare soil	21.26	27.45	37.85	1.241	27.22	0.903
23 February 2016						
Roads	17.55	27.88	37.09	1.919	27.98	1.691
Urban areas	17.67	27.48	37.34	1.902	28.83	1.553
Agricultural	17.35	27.35	37.21	2.156	27.11	1.798
Water	16.09	24.57	33.98	2.472	23.76	1.884
Bare soil	17.97	27.16	36.22	2.458	26.55	2.022
10 March 2016						
Roads	26.64	35.39	42.11	1.959	35.32	1.611
Urban areas	26.64	35.15	43.07	2.040	35.05	1.683
Agricultural	27.23	34.92	41.32	2.193	34.44	1.873
Water	24.08	29.80	41.17	3.659	31.19	3.179
Bare soil	20.87	28.75	38.21	1.819	33.83	1.418

To increase the explanatory capacity of satellite images and to correct the distortion or deterioration to find a more accurate representation of the original scene, different correction steps, before interpretation and analysis, must be performed. Radiometric calibrations that are entirely depending on the characteristics of the sensor were performed using ENVI software in both Landsat and spot images. Removing the influence of the atmosphere is a critical pre-processing step in analyzing images of surface reflectance. For this purpose, thermal Landsat images were atmospherically corrected with the atmospheric correction algorithm used in ENVI and spot imagery was recalculated to the surface reflectance using fast line-of-sight atmospheric analysis

of spectral hypercubes (FLAASH). Also, the water vapor content was determined, and the transmittance of the atmosphere was estimated. After that, all images were geometrically linked using image registration workflow in ENVI software.

Retrieval of brightness temperature from Landsat 8 TIRS images

To approximate and remove the atmospheric effect from thermal infrared images in ENVI software, the algorithm considers the following assumptions: 1) the atmosphere is uniform over all the data scene, 2) there is no reflected down welling radiance, 3) an

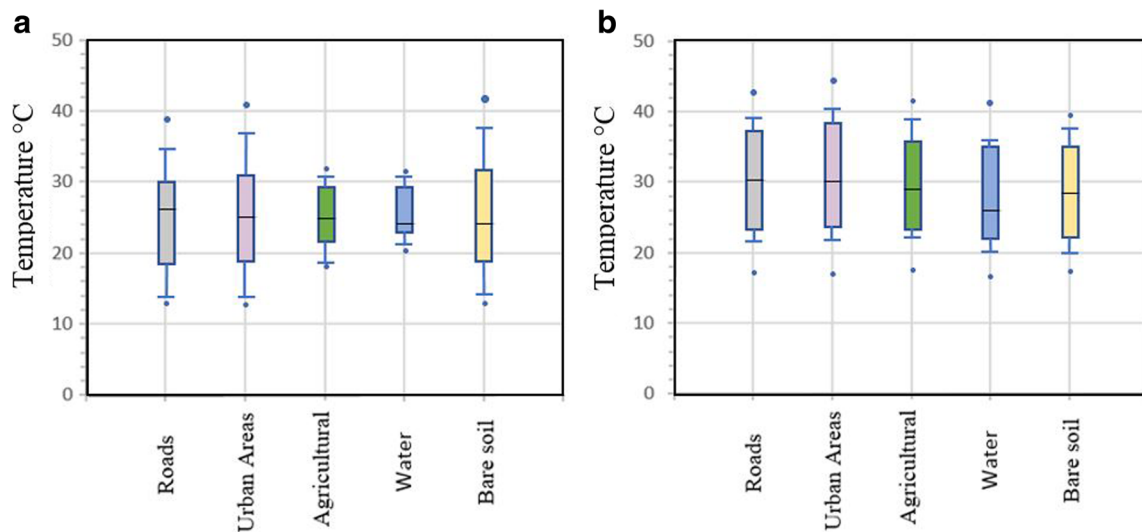


Fig. 5 (a) Boxplots of surface temperature from nighttime images, summer season, (b) Boxplots of surface temperature from daytime images, winter season

existence of a near-blackbody surface exists within the scene, and 4) uniform emissivity for all features. The microwave radiation traveling upward from the top of the atmosphere to the satellite usually represented in Landsat Level-1 data or digital number (DN) can be converted to the top of atmosphere (TOA) brightness temperature using the thermal constants provided in the metadata file. Figure 2 show a typical workflow of the proposed methodology.

The approach to the retrieval of temperature was described in the Landsat 8 User’s Handbook. It is also simplified to two separate steps as follows: first, the DN values were converted to radiance by the following formula:

$$L_{\lambda} = M_L * Q_{cal} + A_L \tag{1}$$

Where:

- L_{λ} spectral radiance ($W/(m^2 * sr * \mu m)$)
- M_L radiance multiplicative scaling factor obtained from the metadata
- A_L radiance additive scaling factor obtained from the metadata
- Q_{cal} the image pixel value

Then, the effective at-satellite temperature of the viewed earth-atmosphere system under the assumption of a uniform emissivity could be obtained, from the above spectral radiance by following formula:

$$T_c = \frac{K2}{\ln\left(\frac{K1}{L_{\lambda}} + 1\right)} - 273.15 \tag{2}$$

Where:

- T_C TOA brightness temperature, in Celsius
- L_{λ} spectral radiance ($Watts/ (m^2 * sr * \mu m)$)
- K1 thermal conversion constant for the band (K1_CONSTANT_BAND_n from the metadata)
- K2 thermal conversion constant for the band (K2_CONSTANT_BAND_n from the metadata)

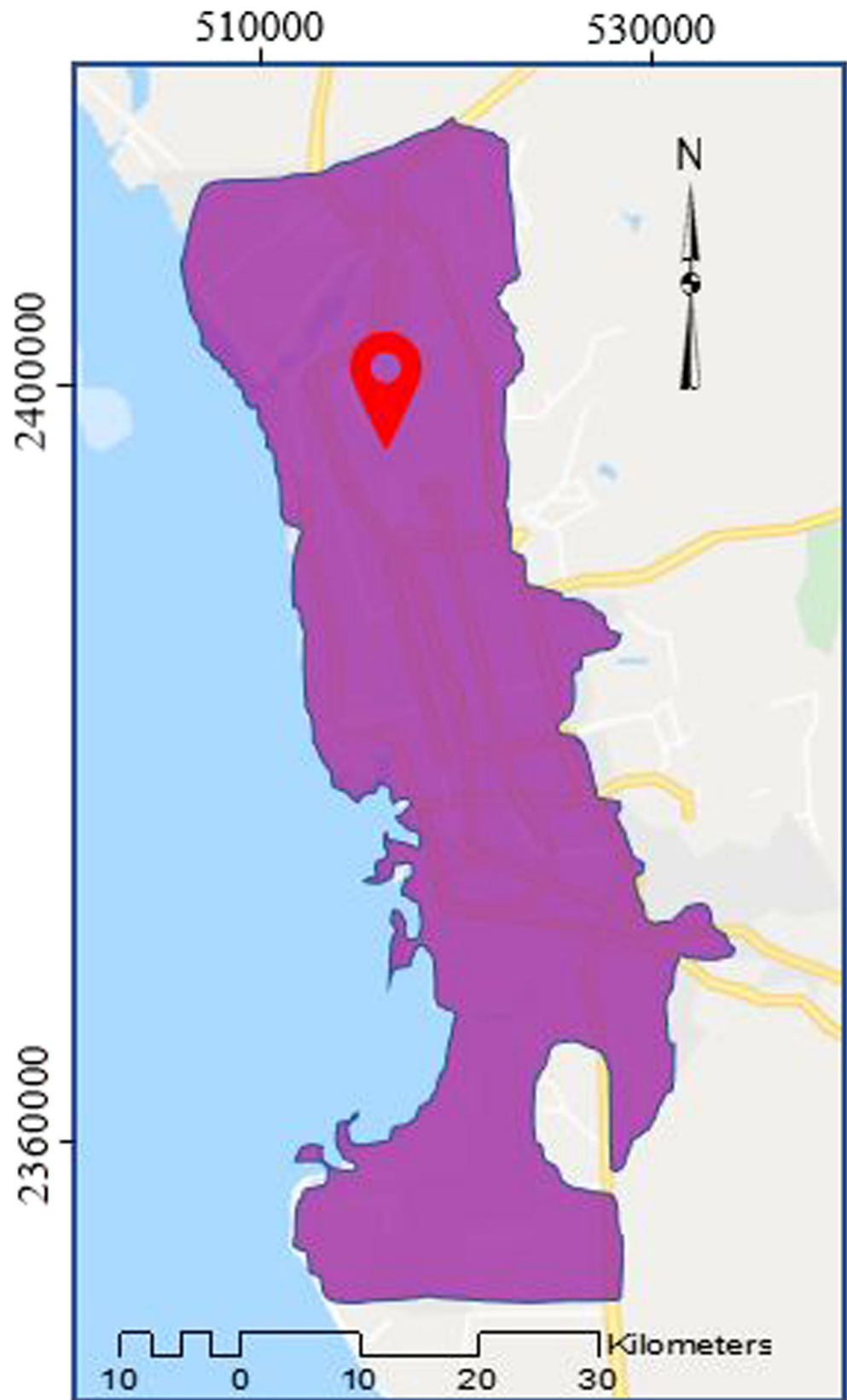
In fact, the radiation emitted from a surface is mainly a function of both the surface temperature and emissivity of that surface material. So, the temperature, T calculated with the assumption listed previously, needs to be modified related to the nature of the surface. For this purpose, information regarding surface emissivity for land cover particularly each class appeared in the scene can be defined after spot image classification and NDVI calculation. Consequently, the true surface temperature can be estimated and SUHI identified.

Spot land cover emissivity calculation and temperature correction

In general, classification process aims to assign each pixel in the digital image into a feature class. However, land cover indicates the physical surface cover of the land, each land cover has its own emissivity which is needed to be linked, as mentioned before, with the extracted temperature for each type. In this study, the classification of Spot imagery was carried out to determine feature types in the scene, also NDVI was estimated over the study area. Based on visual interpretation and field survey, five types of land cover have been determined, i.e., developed, undeveloped areas, vegetation, water, and roads. Supervised classification tool in ENVI software was used to get the area and location for each type.

After that, LSE was estimated and assigned to each pixel. For pixels resulting from the supervised maximum likelihood classification that contain one type of land cover, the emissivity value

Fig. 6 Location of King Abdulaziz airport weather station



was assumed in advance and assigned for each class at wavelength (10.8 μm) according to CBEM (Peres and Da Camara

2005; Snyder et al. 1998) as shown in Table 2. These values were derived from a previous study in which emissivity values were

Table 5 Temperature comparison over King Abdulaziz airport during scenes times

Temperature (°C)	22 June 2015	8 July 2015	24 July 2015	06 Jan. 2016	23 Feb. 2016	10 March 2016
Range obtained from airport station	27–31	30–34	31–39	21–28	19–25	24–31
Calculated by the proposed method	28.13	30.64	37.22	29.13	28.76	35.18

obtained from NOAA-15, emissivity channel-4 (Dash et al. 2005).

For pixels with mixed land cover the emissivity value was calculated according to NBEM (Sobrino and Raissouni 2000; Van de Griend and Owe 1993; Sobrino and Romaguera 2004; Sobrino et al. 2008) and NDVI thresholds method was used for LSE estimation from spot imagery as the following equations:

$$\varepsilon_i = \varepsilon_{v,i}P_v + \varepsilon_{s,i}(1-P_v) + C_i \tag{3}$$

$$P_v = \left[\frac{NDVI - NDVI_{min}}{NDVI_{max} - NDVI_{min}} \right] \tag{4}$$

$$NDVI = \frac{\rho_{IR} - \rho_R}{\rho_{IR} + \rho_R} \tag{5}$$

Where:

- P_v The vegetation fraction
- ρ_{IR} Reflectance value of Infrared channel
- ρ_R Reflectance value of Red channel

According to Yu et al. (2014), emissivities of soil, ε_s and vegetation, ε_v are 0.9668 and 0.9863 respectively and $C = 0$.

The spatial resolution of Landsat developed images is 30 m while in spot imagery, it is 2.5 m. It means that each pixel in Landsat image corresponds approximately to 144 pixels in spot image. In addition, a Landsat pixel presents a single value of apparent temperature calculated for an area about 900 m². However, this area represents different features, with different value of emissivity in the land. In order to recalculate and enhance the temperature value obtained in Eq. 2 according to the emissivity of each feature we will proceed as follow: 1) resampling the Landsat temperature band to a pixel size equals in dimension that of Spot image, i.e., 2.5 m though image registration tool in ENVI software using nearest neighbor algorithm for assigning new values for the produced image. In order to keep the original values of the input Landsat temperature band, the nearest neighbor algorithm was adopted as a resampling technique. This takes the cell center from the input band to determine the closest cell center of the output raster. Also, the nearest neighbor algorithm requires a simple implementation and provides fast time calculation. 2) Matching classified spot image

with the new Landsat resampled image to extract the feature type in each resampled pixel and consequently to assign the emissivity value for each. 3) Recalculating the pixel temperature value obtained by Eq. 2 for the resampled new Landsat image that have 2.5 m pixel size. Hence, it is possible to obtain the LST using the improved mono-window algorithm for LST retrieval from Landsat 8 TIRS Band 10 data as Eqs. 6–8 (Wang et al. 2015; Qin et al. 2001).

$$T_s = [a_{10}(1-C_{10}-D_{10}) + \langle b_{10}(1-C_{10}-D_{10}) + C_{10} + D_{10} \rangle T_{10} - D_{10} T_a] / C_{10} \tag{6}$$

$$C_{10} = \tau_{10} \varepsilon_{10} \tag{7}$$

$$D_{10} = \langle 1 - \tau_{10} \rangle [1 + \langle 1 - \varepsilon_{10} \rangle \tau_{10}] \tag{8}$$

Where

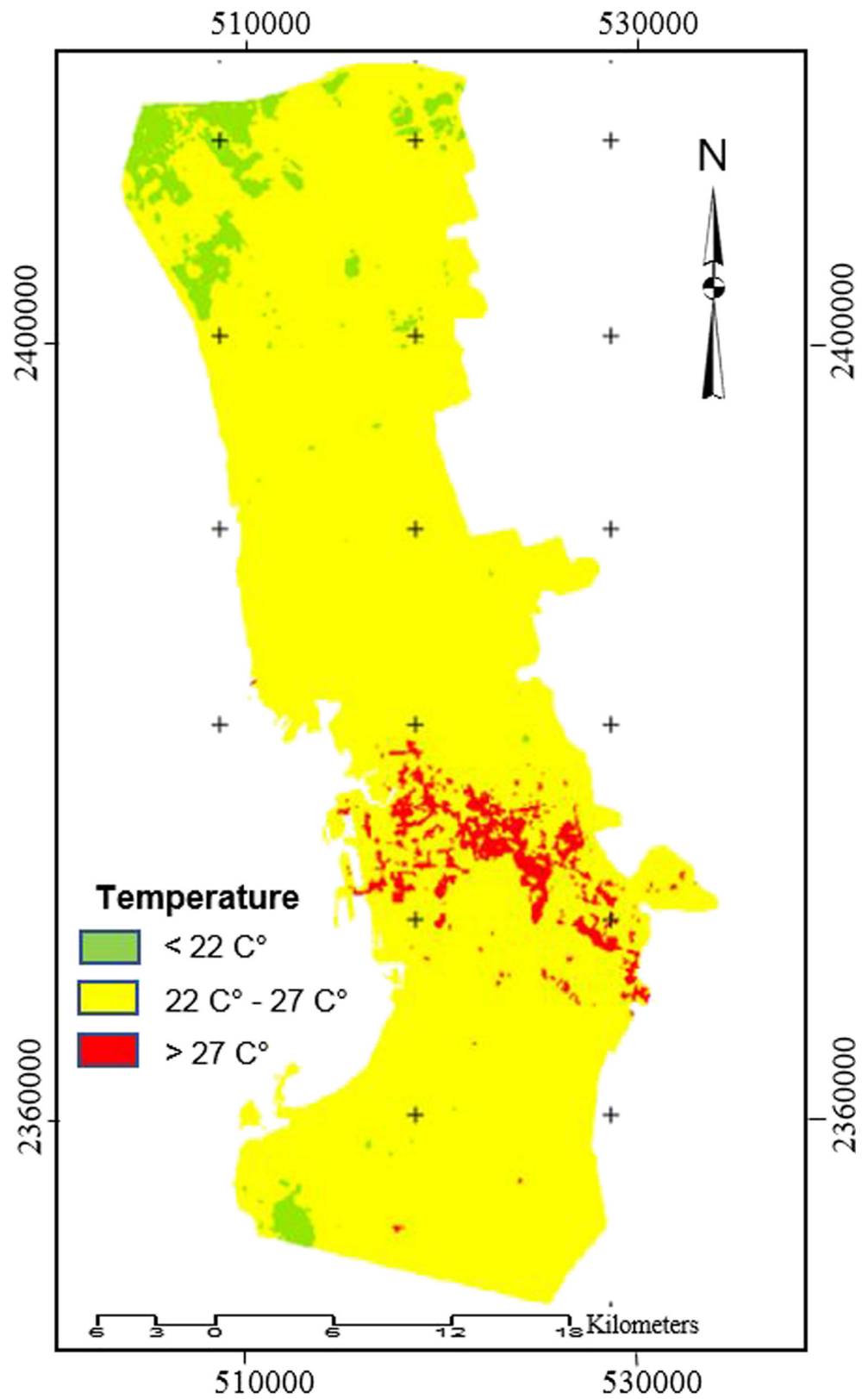
T_s is the LST retrieved from the Landsat 8 TIRS Band 10 data; T_a is the effective mean atmospheric temperature, $T_a = 16.011 + 0.9262T_{10}$ for mid-latitude summer atmosphere model; T_{10} is the brightness temperature of Landsat 8 TIRS band 10; a_{10} and b_{10} are the constants used to approximate the derivative of the Planck radiance function for the TIRS band 10 ($a_{10} = -70.1775$, $b_{10} = 0.4581$ for 20 °C–70 °C temperature range); τ_{10} is atmospheric transmittance of Landsat 8 TIRS Band 10 and ε_{10} is the ground emissivity.

Results and discussion

Spot image classification

The spot image was classified using supervised classification techniques. As mentioned before, five classes consisted of developed areas, undeveloped areas, vegetation, water, and roads were chosen. The maximum likelihood classifier was used to classify the image as shown in Fig. 3. To assess the accuracy of the classification process, 194 testing pixels were assigned in a random way using ENVI software. The coordinates were determined, and a GPS navigator was used to reach the test locations. Overall accuracy, user’s accuracy, producer’s accuracy, and overall kappa coefficient were calculated. Producer’s accuracy for the individual

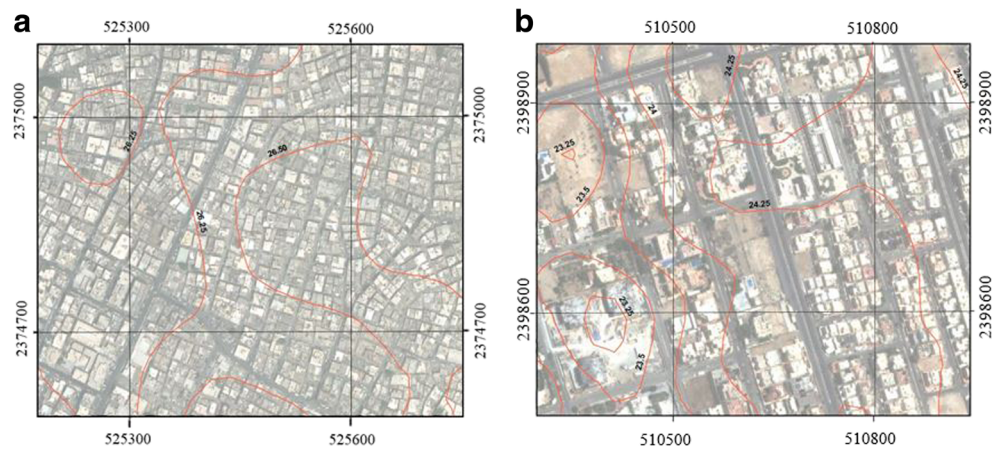
Fig. 7 Average values of LST over Jeddah city during the period from 06/22/2015 to 07/24/2015



classes ranged from 84.21% for undeveloped to 100% for water. The user's accuracy ranged from 64.0% for

undeveloped to 100% for water and vegetation. The kappa estimate was 0.884 (Table 3).

Fig. 8 (a) Random buildings and unplanned neighborhoods in the south of Jeddah, (b) Planned urban neighborhoods in the North of Jeddah



Land surface temperature retrieval

Spatial distribution of the LST over Jeddah city using classification-based emissivity and NDVI-based emissivity is shown in Fig. 4. In addition, the Table 4 shows land cover temperature derived from Landsat 8 images used in the study. In summer season, roads in the city recorded average temperatures higher than other areas, with a mean average

temperature of 24.75 °C. The highest road temperatures were concentrated in the south of Jeddah, the maximum roads temperature was 38.80 °C. The mean average temperature of urban areas and agricultural land are approximately the same, they were 24.38 °C and 24.39 °C respectively. The highest temperature for urban areas was in Southern Jeddah at a maximum temperature of 40.86 °C, while the highest temperature of agricultural land was in northern Jeddah at a maximum

Fig. 9 SUHIs over Petromin neighborhood, Jeddah, KSA

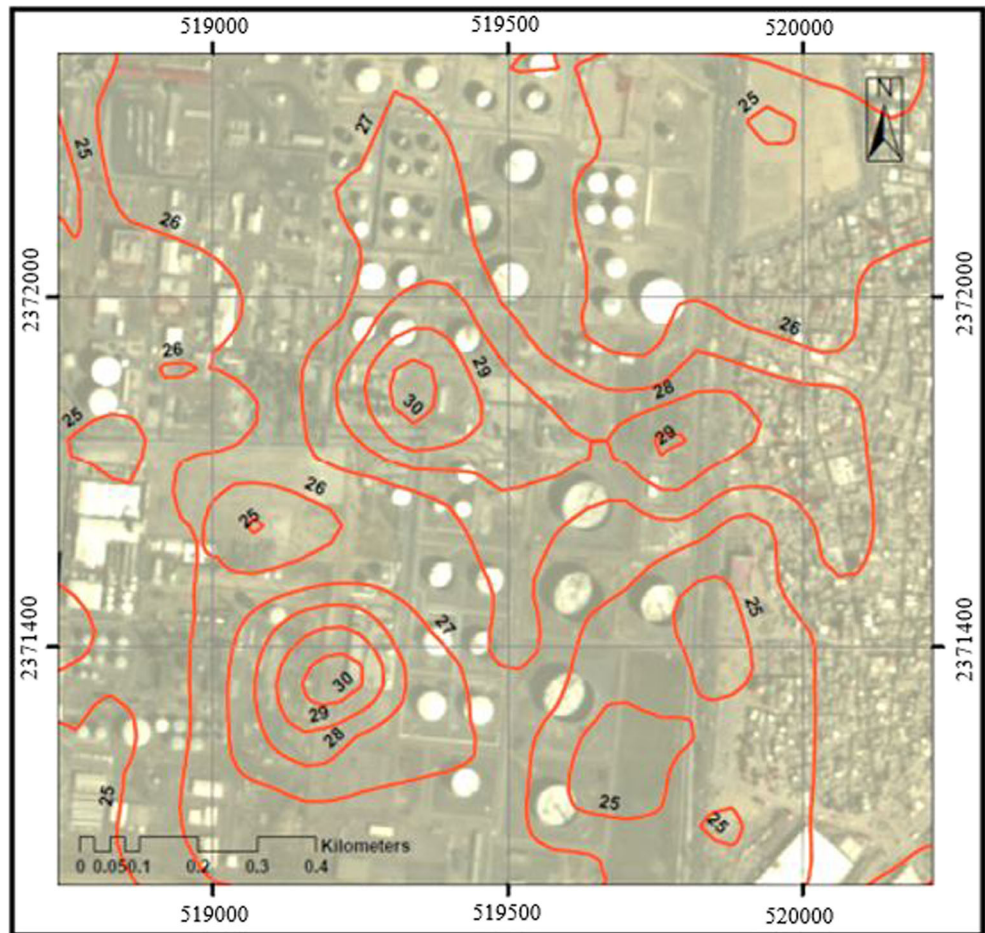
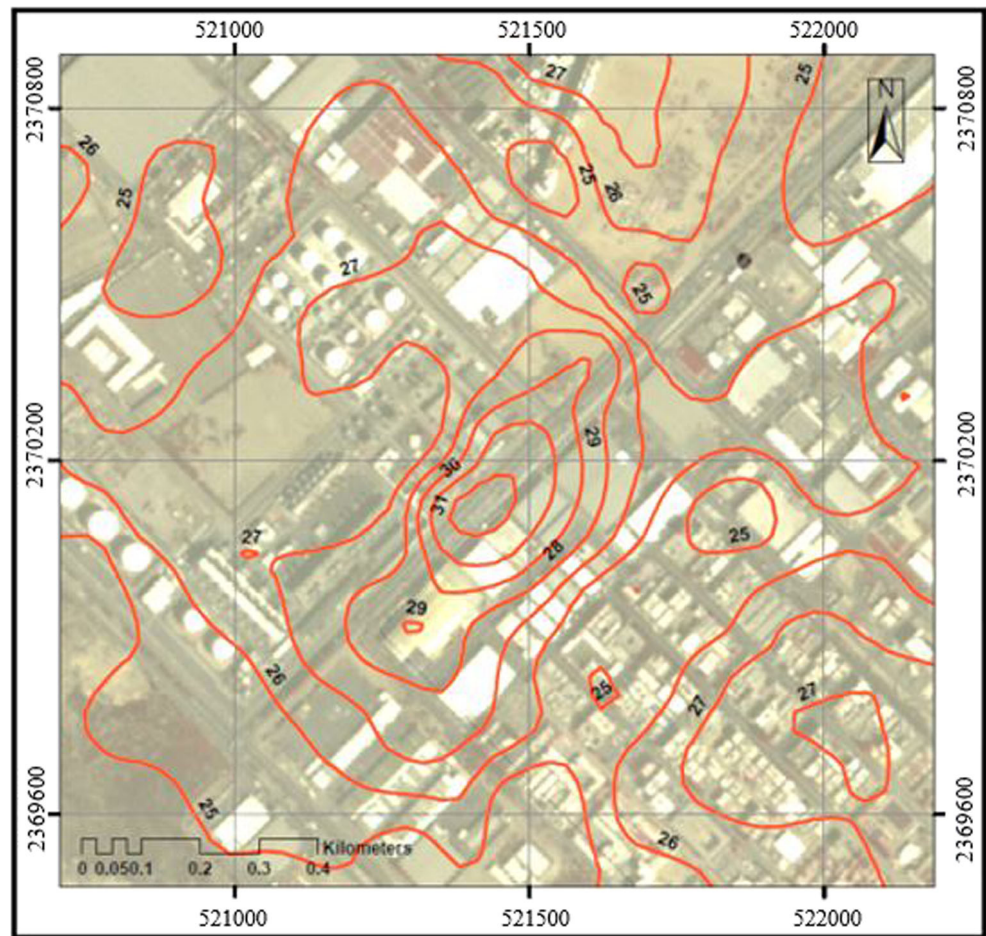


Fig. 10 SUHI over Almohajer neighborhood, Jeddah, KSA



temperature of 32.18 °C. The mean average temperature of water in Jeddah was 24.00 °C while its highest value was 31.20 °C. Bare soil recorded a mean average temperature of 23.93 °C which is lower than other areas, while the maximum temperature was concentrated in south and central Jeddah and recorded 42.63 °C. In winter season, it could be found that LST ranged between 16.09 °C and 43.06 °C. The highest temperature was recorded from roads and urban areas, while the lowest temperature comes from the water surface. The vegetation areas recorded a mean average temperature of 29.93 °C.

However, the mean can be affected by outliers and moves towards them. Therefore, it is necessary to see if there are outliers inside the population or not. To do so, standard deviation, median, normalized mean absolute deviation were computed and presented in Table 4. Also, Fig. 5 presents boxplots of surface temperature for each class, Fig. 5(a) for nighttime Landsat images during the period from 06/22/2015 to 07/24/2015, and Fig. 5(b) for daytime Landsat images during the period from 01/06/2016 to 03/10/2016.

To check the accuracy of the proposed method, past temperature information obtained from the meteorological station

located in King Abdulaziz airport and available online was compared with the obtained results from the proposed method over the same place during scenes times. King Abdulaziz airport station, see Fig. 6, provides hour by hour information about temperature. However, for archiving purposes, the temperature is presented four times a day (King Abdulaziz airport weather station information 2018). So, the range of temperature presented in the period from 6:00 a.m. to 12:00 p.m. was used to compare with daytime images, while the range from 6:00 p.m. to 00:00 a.m. was used to compare with nighttime images. Table 5 shows the comparison between range of temperature obtained from airport station and the temperature value calculated by the proposed method over King Abdulaziz airport during the scene time.

Figure 7 shows the average values of LST over the study area. This figure highlights pixels that have difference LST more than 5 degrees with the surroundings during the period from 06/22/2015 to 07/24/2015. The spatial location of areas that recorded high temperatures is in the Southern region of Jeddah city (Petromin, Al Mohajer, Industry city, Al-Gamaa, and Madain Al-Fahd Neighborhood). The appeared areas are small in size and have irregular shapes.

SUHI over Jeddah city

It is clear from the previous results that surface urban heat islands are concentrated in the south of Jeddah city. In these areas, random buildings and unplanned neighborhoods as shown in Fig. 8(a) contributed to the increase of temperature through narrow streets and alleys that prevent the flow of air in an appropriate way. In addition, factories and waste incineration in the south of Jeddah contributes to the increase the temperature compared to the north and center of Jeddah as shown in Fig. 8(b). The north and center of Jeddah have good urban planning in addition to the effect of the sea breeze, which has a clear influence in reducing temperatures.

For the SUHIs over Petromin neighborhood as shown in Fig. 9, there are two adjacent peaks located in the center of neighborhood (about 1.60 km away from the Red Sea). The first peak covers an area about 0.12 km² with a maximum temperature of 30 °C. The second peak covered an area of about 0.34 km² and the maximum temperature reached also 30 °C. The range, difference in temperature between the peak and the margin, was 4 °C.

In Almohajer neighborhood, where there are a lot of factories and industrial places, the SUHI is located in the east of the neighborhood as shown in Fig. 10. That SUHI is far about 3.7 km from the Red Sea and it has an area of about 0.32 km². The maximum temperature reached 31 °C, and the range was 5 °C.

Conclusions

In this work, a satellite-based map for SUHIs over Jeddah city during summer 2015 was produced. Night vision Landsat 8 TIRS images (band 10) were used. LST were estimated using the improved mono-window algorithm. The ground emissivity was estimated through the land cover pattern from spot 5 data. Based on the results of this study, the SUHIs over Jeddah city appeared as small boundaries in the south of the city. This configuration is due to the land use patterns. The differences in nighttime surface temperatures between urban and non-urban areas ranges from 4 to 7 °C. It is important to mention that night vision Landsat 8 imagery has proved its efficiency in delineating SUHIs. In addition, it allows monitoring the behavior, movement, and size of these UHIs. Hence, it is possible for the researcher to perform many different environmental studies related to urban planning. Additionally, for most situations, study of surface urban heat island phenomena through satellite data is more accurate than its study through traditional ground observation data. In fact, unlike traditional terrestrial observation methods, satellite images collect data for different regions simultaneously.

References

- Abu-Hamdeh NH (2003) Thermal properties of soils as affected by density and water content. *Biosyst Eng* 86(1):97–102
- Abutaleb K, Ngie A, Darwish A, Ahmed M, Arafat S, Ahmed F (2015) Assessment of urban heat island using remotely sensed imagery over Greater Cairo, Egypt. *Adv Remote Sens* 4:35–47
- Barducci A, Pippi I (1996) Temperature and emissivity retrieval from remotely sensed images using the ‘grey body emissivity’ method. *IEEE Trans Geosci Remote Sens* 34:681–695
- Barsi JA, Schott JR, Hook SJ, Raqueno NG, Markham BL, Radocinski RG (2014) Landsat-8 thermal infrared sensor (tirs) vicarious radiometric calibration. *Remote Sens* 6(11):607–11,626
- Becker F, Li Z-L (1990) Temperature-independent spectral indices in thermal infrared bands. *Remote Sens Environ* 32:17–33
- Berdahl P, Bretz S (1997) Preliminary survey of the solar reflectance of cool roofing materials. *Energy Build* 25:149–158
- Bhargava A, Lakmini S, Bhargava S (2017) Urban heat island effect: it’s relevance in urban planning. *J Biodivers Endanger Species* 5(1):1, 000,187
- Bonafoni S, Anniballe R, Pichierri M (2015) Comparison between surface and canopy layer urban heat island using MODIS data. *Urban Remote Sensing Event (JURSE), Lausanne*. <https://doi.org/10.1109/JURSE.2015.7120457>
- Borel CC (1997) Iterative retrieval of surface emissivity and temperature for a hyperspectral sensor. In *First JPL workshop on remote sensing of land surface Emissivity, Pasadena, CA, May 6–8, 1–5*.
- Brazel AJ, Selover N, Vose R, Heisler G (2000) The tale of two climates: Baltimore and Phoenix urban LTER sites. *Clim Res* 15:123–135
- Cristóbal J, Jiménez-Muñoz JC, Sobrino JA, Ninyerola M, Pons X (2009) Improvements in land surface temperature retrieval from the Landsat series thermal band using water vapor and air temperature. *J Geophys Res* 114:D08103. <https://doi.org/10.1029/2008JD010616>
- Cristóbal J, Jiménez-Muñoz JC, Prakash A, Mattar C et al (2018) An Improved single-channel method to retrieve land surface temperature from the Landsat-8 thermal band. *Remote Sens* 10(3):431
- Dash P, Gfittsche F-M, Olesen F-S, Fischer H (2005) Separating surface emissivity and temperature using two-channel spectral indices and emissivity composites and comparison with a vegetation fraction method. *Remote Sens Environ* 96:1–17
- Fortuniak K (2009). Global environmental change and urban climate in Central European cities. *International Conference on Climate Change, the environmental and socioeconomic response in the southern Baltic region. Szczecin, Poland, 25 - 28 May 2009*
- Future Saudi cities, Jeddah CPI profile (2018) <https://www.future Saudicities.org/cpi-reports/CPI%20Profile%20for%20Jeddah.pdf>. Accessed 10 Mar 2018
- He JF, Liu JY, Zhuang DF, Zhang W, Liu ML (2007) Assessing the effect of land use/land cover change on the change of urban heat island intensity. *Theor Appl Climatol* 90(3–4):217–226
- Jiménez-Muñoz JC, Sobrino JA (2003) A generalized single-channel method for retrieving land surface temperature from remote sensing data. *J Geophys Res* 108(D22):4688. <https://doi.org/10.1029/2003JD003480>
- Kahle AB, Madura DP, Soha JM (1980) Middle infrared multispectral aircraft scanner data: analysis for geological applications. *Appl Opt* 19:2279–2290
- King Abdulaziz airport weather station information (2018) Available online: <https://www.timeanddate.com/weather/saudi-arabia/jeddah/historic>. Accessed 15 Oct 2018
- Li Z-L, Petitcolin F, Zhang RH (2000) A physically based algorithm for land surface emissivity retrieval from combined mid-infrared and thermal infrared data. *Sci China Ser E* 43:23–33

- Li J, Li J, Weisz E, Zhou DK (2007) Physical retrieval of surface emissivity spectrum from hyperspectral infrared radiances. *Geophys Res Lett* 34:L16812
- Li Z-L, Wu H, Wang N, Qiu S, Sobrino JA, Wan Z, Tang B-H, Yan G (2012) Land surface emissivity retrieval from satellite data. *Int J Remote Sens* 34:3084–3127
- Li Z-L, Wu H, Wang N, Qiu S, Sobrino JA, Wan Z, Tang B-H, Yan G (2013) Land surface emissivity retrieval from satellite data. *Int J Remote Sens* 34(9–10):3084–3127
- Ma XL, Wan ZM, Moeller CC, Menzel WP, Gumley LE, Zhang YL (2000) Retrieval of geophysical parameters from moderate resolution imaging spectroradiometer thermal infrared data: evaluation of a two-step physical algorithm. *Appl Opt* 39:3537–3550
- Montanaro M, Gerace A, Lunsford A, Reuter D (2014) Stray light artifacts in imagery from the Landsat 8 thermal infrared sensor. *Remote Sens* 6:10,435–10,456 14
- Oke TR (1982) The energetic basis of the urban heat island. *Q J R Meteorol Soc* 108(455):1–24
- Oke TR (1987) *Boundary layer climates*. Routledge, London
- Oke TR, Mills G, Christen A, Voogt JA (2017) *Urban climates*. Cambridge University Press, Cambridge
- Parlow E, Vogt R, Feigenwinter C (2014) The urban heat island of Basel—seen from different perspectives. *Journal of the Geographical Society of Berlin ERDE* 145(1–2):96–110
- Peres LF, Da Camara CC (2005) Emissivity maps to retrieve land-surface temperature from MSG/SEVIRI. *IEEE Trans Geosci Remote Sens* 43:1834–1844
- Qin Z, Kameli A, Berliner P (2001) A mono-window algorithm for retrieving land surface temperature from Landsat TM data and its application to the Israel-Egypt border region. *Int J Remote Sens* 22:3719–3746
- Salisbury JW, D’Aria DM (1992) Emissivity of terrestrial materials in the 8–14 μm atmospheric window. *Remote Sens Environ* 42:83–106
- Salleh SA, Abd.Latif Z, Mohd WMNW, Chan A (2013) Factors contributing to the formation of an urban heat island in Putrajaya, Malaysia. *Procedia Soc Behav Sci* 105:840–850
- Sinasi K, Umut Gul B, Mehmet K, Dursun Zafer S (2012) Assessment of urban heat islands using remotely sensed data. *Ekoloji* 21(84):107–113
- Snyder WC, Wan Z, Zhang Y, Feng YZ (1998) Classification-based emissivity for land surface temperature measurement from space. *Int J Remote Sens* 19:2753–2774
- Sobrino JA, Raissouni N (2000) Towards remote sensing methods for land cover dynamic monitoring: application to Morocco. *Int J Remote Sens* 21:353–366
- Sobrino JA, Romaguera M (2004) Land surface temperature retrieval from MSG1-SEVIRI data. *Remote Sens Environ* 92:247–254
- Sobrino JA, Jimenez-Muoz JC, Soria G, Romaguera M, Guanter L, Moreno J, Plaza A, Martinez P (2008) Land surface emissivity retrieval from different VNIR and TIR sensors. *IEEE Trans Geosci Remote Sens* 46:316–327
- United States Geological Survey (2017) Landsat 8 operational land imager and Thermal infrared sensor calibration notices. Available online: http://landsat.usgs.gov/calibration_notices.php. Accessed 13 Jan 2017
- USGS Global Visualization Viewer (2017) Available online: <http://glovis.usgs.gov>. Accessed 24 June 2017
- Van de Griend AA, Owe M (1993) On the relationship between thermal emissivity and the normalized difference vegetation index for natural surfaces. *Int J Remote Sens* 14:1119–1131
- Voogt JA, Oke TR (2003) Thermal remote sensing of urban climates. *Remote Sens Environ* 86:370–384
- Wan ZM, Li Z-L (1997) A physics-based algorithm for retrieving land-surface emissivity and temperature from EOS/MODIS data. *IEEE Trans Geosci Remote Sens* 35:980–996
- Wang F, Qin Z, Song C, Tu L, Kameli A, Zhao S (2015) An improved mono-window algorithm for land surface temperature retrieval from Landsat 8 thermal infrared sensor data. *Remote Sens* 7:4268–4289. <https://doi.org/10.3390/rs70404268>
- Ward D (2008) Urban heat islands. http://www.windows.ucar.edu/tour/link=/earth/climate/urban_heat_islands.html. Accessed 10 Mar 2018
- Watson K (1992) Two-temperature method for measuring emissivity. *Remote Sens Environ* 42:117–121
- Yu X, Guo X, Wu Z (2014) Land surface temperature retrieval from landsat 8 tirs—comparison between radiative transfer equation-based method, split window algorithm and single channel method. *Remote Sens* 6:9829–9852
- Zhou B, Rybski D, Kropp JP (2013) On the statistics of urban heat island intensity. *Geophys Res Lett* 40:5486–5491. <https://doi.org/10.1002/2013GL057320>